Nonlinear analysis of the coupling between interface deflection and hexagonal patterns in Rayleigh-Bénard-Marangoni convection

Layachi Hadji
Department of Mathematics, The University of Alabama, Tuscaloosa, Alabama 35487
(Received 19 January 1996)

An analytical study is conducted to examine the coupling between buoyancy and surface tension forces in a shallow pool of a Boussinesq fluid. The liquid layer is bounded below by a rigid and poorly conducting plate, and is open to the air at its upper deformable free surface. At the onset of convection, the coupling between buoyancy and surface-tension-induced instabilities is represented by a single parameter m. A pattern selection study predicts the existence of a critical value for the parameter m, m_c, that separates subcritical hexagons with upflow at their centers from subcritical hexagons with downflow at their centers. Several experimental situations are identified in terms of the Prandtl, Galileo, and capillary numbers, and the dependence of m_c on these parameters is analyzed. Further, expressions for the interface deflection that accompanies the onset of Rayleigh-Bénard-Marangoni convection are derived. These expressions show explicitly the dependence of the interface morphology on the coupling parameter m and on the Prandtl, Galileo, and capillary numbers. It is also noted that, for a specific set of experimental parameters, spatial resonance will occur which leads to a situation in which the interfacial deformations do not conform to the flow pattern. [S1063-651X(96)10906-5]

PACS number(s): 47.20.Bp, 47.20.Dr, 47.54.+r, 47.27.Te

I. INTRODUCTION

Rayleigh-Bénard-Marangoni (RBM) convection refers here to the spatially periodic flows induced by the coupled effects of buoyancy and surface tension forces in a shallow pool of fluid heated from below, and whose upper surface is free and deformable. This convection process is now widely recognized for its practical significance due to the fact that it is omnipresent in a large variety of industrial processes, notably crystal growth experiments, film coating processes, and low gravity fluid experiments.

The phenomenon of surface-tension-driven cellular convection was brought to light by Pearson [1], some six decades after the experimental findings of Bénard [2]. Pearson's study was stimulated by the remarks of Jeffreys [3] and the experimental work of Block [4]. These investigations were later improved by Scriven and Sternling [5], who included the effects of interface deformation. Nield [6] investigated the dual effects of surface tension and buoyancy on the linear stability of the conduction state for the case of a nondeforming free surface. Most recent studies deal primarily with the influence of the interfacial deflection on the stability of the motionless state. These studies are based on the linearized set of equations and boundary conditions (see Benguria and Depassier [7], and references therein). A numerical three-dimensional nonlinear analysis of RBM convection has been performed by Kraska and Sani [8]. These authors derive a set of seven equations for the marginal amplitudes that describe the evolution of the convective state near linear threshold. These amplitudes appear in the representation of the planform function which has been chosen to include the patterns of sheets, rectangles, hexagons, and other mixed states. A stability analysis is then undertaken to isolate the stable pattern as a function of the main parameters of the problem, namely the Prandtl, Marangoni, Rayleigh, and capillary numbers. Further, they present results pertaining to the shape of the free surface.

In this work, a weakly nonlinear study of RBM convection is conducted. Most aspects of our model are the same as those formulated by Kraska and Sani [8], but with the exception that a lower boundary of low thermal conductance is assumed. The method of analysis is also different: The critical wavelength at the onset of convection becomes infinitely long in the limit of a system that is nearly insulating. Using long wavelength asymptotics, we model the three-dimensional RBM problem by a set of three nonlinear coupled evolution equations for the leading order perturbations of the temperature, vertical component of vorticity, and interfacial deflection. The type of hexagonal pattern that is observed near threshold is determined by conducting a stability analysis directly from the derived equations. Our method yields analytical expressions for the fields, the critical parameters, and the interface shape, from which we assess the relative importance of the different physical parameters that govern RBM convection. Only two studies dealing primarily with the question of interface deflection stand out: a theoretical analysis by Perez-Garcia *et al.* [9] and an experimental study by Cerisier *et al.* [10]. Their main findings may be summed up as follows: At the center of the hexagonal cell, upflow is associated with a bump in the buoyancy case and a trough in the surface tension case. The analysis of Perez-Garcia *et al.* [9], being linear, does not take into account the direction of the flow and the experimental work of Cerisier *et al.* [10], being carried out using only a single fluid is unable to identify the dependence upon the Prandtl number. These results are also in agreement with the predictions of Kraska and Sani [8]. These authors have only mentioned, without elaboration, some anomalous behavior of the interface deflection for low Prandtl numbers. Our inquiry into the forms which the free surface can assume under the influence of the combined motion of buoyancy and thermocapillarity shows that the interface deflection, besides being dependent upon the relative strength of buoyancy and surface tension

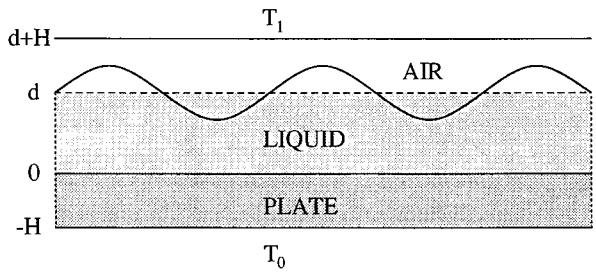

FIG. 1. Sketch of a liquid layer of depth d underlying a layer of air of depth H. The lower plate has a thickness H, and is assumed to have the same thermal conductance as that of air. The free air-liquid surface is planar (dotted line) in the motionless state, and deformable (continuous line) in the convective state. T_1 and T_0 are the upper and lower temperatures, respectively.

forces, is also a function of the type of hexagonal pattern which is determined by a stability analysis in the parameter space of the problem consisting of the Prandtl, capillary, and Galileo numbers.

The content of the paper is outlined in the following: In Sec. II the mathematical formulation of the problem is presented. In Sec. III the method of solution is introduced, and closed form expressions for the temperature, velocity, and critical parameters are found. The lengthy algebraic expressions have been verified using the mathematical software MACSYMA. The stability analysis of the planform of convection and the determination of the interface deflection are carried in Sec. IV and some remarks and the conclusion are presented in Sec. V.

II. FORMULATION OF THE PROBLEM

Consider a shallow liquid layer of height d that is bounded below by a rigid plate of thermal conductance k_p and thickness H. A layer of air, of thickness H, is allowed to exist between the liquid and a top plate whose thermal conductance is assumed to be high. The free air-liquid interface, which separates the air and liquid layers, deforms only when the liquid is in motion. An upward heat flux $\mathcal{F}$ is imposed through the whole system by a suitable control of the temperatures at the outer sides of the plates T_0 and T_1. Figure 1 shows a schematic diagram of the experimental setup. Within the Boussinesq approximation, the governing equations for the conservation of momentum, heat, and mass are described by

$$\frac{\partial \mathbf{u}}{\partial t}+\mathbf{u}\cdot\boldsymbol{\nabla}\mathbf{u}=-(1/\rho)\boldsymbol{\nabla}p+[1-\alpha_T(T-T_0)]\mathbf{g}+\nu\nabla^2\mathbf{u}, \tag{2.1}$$

$$\frac{\partial T}{\partial t}+\mathbf{u}\cdot\boldsymbol{\nabla}T=\kappa\nabla^2 T, \tag{2.2}$$

$$\boldsymbol{\nabla}\cdot\mathbf{u}=\mathbf{0}. \tag{2.3}$$

The fluid has a thermal diffusivity κ, a constant reference density ρ, a dynamic viscosity ν, and a thermal expansivity α_T. The other symbols that appear in Eqs. (2.1)–(2.3) are the velocity $\mathbf{u}$, the temperature T; the pressure p, the gravitational vector field $\mathbf{g}=-g\mathbf{k}$, $\mathbf{k}$ being a unit vector in the upward direction; the gradient vector $\boldsymbol{\nabla}$; and a reference temperature T_0.

We complete the description of the system by supplementing Eqs. (2.1)–(2.3) by appropriate boundary conditions. The no-slip condition is assumed to hold at the lower rigid plate located at $Z=0$.

$$\mathbf{u}=\mathbf{0}. \tag{2.4}$$

At the planar and rigid interface between the liquid and the lower plate, the continuity of temperature and heat flux yield

$$T=T_P, \quad \frac{\partial T}{\partial Z}=\beta\frac{\partial T_p}{\partial Z} \quad \text{on } Z=0, \tag{2.5}$$

where β represents the ratio of the thermal conductivity of the lower plate to that of the liquid ($\beta\ll 1$), and T_p is the temperature in the plate which satisfies the heat conduction equation

$$\frac{\partial T_p}{\partial t}=\kappa_p\nabla^2 T_p. \tag{2.6}$$

At the air-liquid interface, located at $Z=d+\eta(X,Y,t)$, where $\eta(X,Y,t)$ represents the deviation from planarity, the stress balance equation, written in tensor notation, takes the form (Levitch and Krylov [11])

$$\left[(p-p_a)+\sigma\left(\frac{1}{\mathcal{R}_1}+\frac{1}{\mathcal{R}_2}\right)\right]n_i=\mu\left[\frac{\partial v_i}{\partial x_k}+\frac{\partial u_k}{\partial x_i}\right]-\frac{\partial\sigma}{\partial x_i}, \tag{2.7}$$

where p and p_a are the pressures at the liquid side and the air side, respectively; σ is the surface tension; $\mathcal{R}_1$ and $\mathcal{R}_2$ are the principal radii of curvature of the interface and n_i; ($i=1, 2, 3$) are the components of the outward unit vector normal to the interface $\mathbf{n}$, whose norm is denoted by N,

$$\mathbf{n}=(-\eta_X,-\eta_Y,1)/N, \quad N=(1+\eta_X^2+\eta_Y^2)^{1/2}. \tag{2.8}$$

Equation (2.7) translates into the following for the normal stress balance:

$$\begin{aligned} p-p_a=&\frac{2\mu}{N}[u_X(\eta_X)^2+(u_Y+v_X)\eta_X n_Y-(u_Z+w_X)\eta_X \\ &+v_Y(\eta_Y)^2-(v_Z+w_Y)\eta_Y+w_Z] \\ &-\frac{\sigma}{N\sqrt{N}}[\eta_{XX}+\eta_{YY}], \end{aligned} \tag{2.9}$$

where u, v, and w are the components of the velocity vector $\mathbf{u}$; the subscripts X and Y correspond to differentiation with respect to X and Y, respectively; μ is the viscosity; and ∇_H denotes the horizontal gradient. The tangential stresses balance, from Eq. (2.7), implies

$$\frac{\mu}{N}[-2u_X\eta_X(1+\eta_Y^2)+(u_Y+v_X)\{-\eta_Y(1+\eta_Y^2)+\eta_Y\eta_X^2\}$$
$$+(u_Z+w_X)(1+\eta_Y^2-\eta_X^2)+2v_Y\eta_X\eta_Y^2-2\eta_X\eta_Y(v_Z$$
$$+w_Y)+2w_Z\eta_X]=[\sigma_X-\eta_X\eta_Y\sigma_Y+\eta_X\sigma_Z] \quad (2.10a)$$

and

$$\frac{\mu}{\sqrt{N}}[-\eta_X(v_X+u_Y)-2\eta_Y v_Y+(v_Z+w_Y)(1-\eta_Y^2)$$
$$-(w_X+u_Z)\eta_X\eta_Y+2w_Z\eta_Y]=[\sigma_Y+\eta_Y\sigma_Z], \quad (2.10b)$$

and finally the free surface kinematic boundary condition, which also connects the interface perturbations to the fluid velocity, yields

$$w=un_X+v\eta_Y+\frac{\partial\eta}{\partial t}. \quad (2.11)$$

The continuity of temperature and heat flux at the free surface imply

$$T=T_a, \quad \mathbf{n}\cdot\nabla(kT-k_aT_a)=0 \quad \text{on} \quad Z=d+\eta, \quad (2.12)$$

where T_a is the temperature in the air layer, and where k and k_a are the thermal conductivities of the liquid and air, respectively.

The system possesses a basic state defined by a motionless fluid in which heat transfer is by conduction alone. The temperature profile is linear and varies only in the vertical direction,

$$T_B(Z)=\mathcal{F}(Z-d)+T_R, \quad (2.13a)$$

$$T_R=T_1-\mathcal{F}H/\beta, \quad \mathcal{F}=\frac{\beta(T_1-T_0)}{d\beta+2H}, \quad (2.13b)$$

$$p_B(Z)=p_a-g\rho_0\{(Z-d)+\alpha_T(\mathcal{F}/2)(Z-d)^2\}. \quad (2.13c)$$

All quantities are nondimensionalized in the standard way: length is scaled by d, time by d^2/κ, and temperature by $\mathcal{F}d$. Upon subtraction of the basic state, the following system of equations and corresponding boundary conditions is obtained for the convective variables:

$$P^{-1}\left[\frac{\partial\mathbf{u}}{\partial t}+\mathbf{u}\cdot\nabla\mathbf{u}\right]=-\nabla p+R\theta\mathbf{k}+\nabla^2\mathbf{u}, \quad (2.14)$$

$$\frac{\partial\theta}{\partial t}+\mathbf{u}\cdot\nabla\theta=\nabla^2\theta+w, \quad (2.15)$$

$$\nabla\cdot\mathbf{u}=\mathbf{0}, \quad (2.16)$$

where θ is the temperature fluctuation, and R and P, respectively, are the Rayleigh and Prandtl numbers,

$$R=\frac{\alpha_T g d^4\mathcal{F}}{\nu\kappa}, \quad P=\frac{\nu}{\kappa}. \quad (2.17)$$

At the free surface, the convective perturbations for the normal and tangential stresses balance equations satisfy

$$p-GP\eta+(R/2)\eta^2+(2/N)[u_X(\eta_X)^2+\eta_X\eta_Y(u_Y+v_X)$$
$$-(u_Z+w_X)\eta_X+v_Y(\eta_Y)^2-\eta_Y(v_Z+w_Y)+w_Z]$$
$$=N^{-3/2}[\eta_{XX}+\eta_{YY}][1/C+M(\eta-\theta)], \quad (2.18)$$

$$(1/N)[-2u_X\eta_X(1+\eta_Y^2)-2\eta_Y(u_Y+v_X)(1+\eta_Y^2-\eta_X^2)$$
$$+(u_Z+w_X)(1+\eta_Y^2-\eta_X^2)+2v_Y\eta_X\eta_Y^2-2\eta_X\eta_Y(v_Z$$
$$+w_Y)+2w_Z\eta_X]=M[-\theta_X(1+\eta_Y^2)+\eta_X\eta_Y\theta_Y+\eta_X$$
$$-\eta_X\theta_Z], \quad (2.19)$$

$$N^{-1/2}[-\eta_X(v_X+u_Y)-2\eta_Y v_Y+(1-\eta^2)(v_Z+w_Y)$$
$$-\eta_X\eta_Y(w_X+u_Z)+2w_Z\eta_y]=M(\eta_Y-\theta_Y-\eta_Y\theta_Z). \quad (2.20)$$

The conditions of continuity of the temperature and of the heat flux at the free surface are combined to yield the following boundary condition relating the temperature and interface convective perturbations:

$$\mathbf{n}\cdot\nabla\theta=-\beta'(\eta-\theta), \quad (2.21)$$

where β' is a heat transfer Biot number which depends upon the thermal conductivities of air and of the top plate that bounds it from above, on the thicknesses of the plate and air layer and on the wave number at the onset of convection. The reader is referred to Hadji, Safar, and Schell [12] for a detailed calculation of β'.

In deriving Eqs. (2.18)–(2.21), we have assumed that the surface tension varies linearly with temperature,

$$\sigma=\sigma_0+\Gamma(T-T_0), \quad \Gamma=-\frac{\partial\sigma}{\partial T}. \quad (2.22)$$

The dimensionless parameters that appear in Eqs. (2.18)–(2.20) are the Marangoni number M, the Galileo number G, and the capillary number C, whose definitions are

$$M=\frac{\Gamma\mathcal{F}d^2}{\rho\nu\kappa}, \quad G=\frac{gd^3}{\nu^2} \quad \text{and} \quad C=\frac{\nu\kappa\rho}{\sigma_0 d}. \quad (2.23)$$

The Marangoni number expresses the competition between the destabilizing forces due to surface tension gradients and the stabilizing forces due to viscous drag and heat dissipation. The Galileo number represents the competition between the gravitational effects and viscous drag. Small Galileo numbers pertain to thin and viscous fluid layers or to microgravity situations, while large Galileo numbers correspond to situations involving thicker and less viscous fluids under terrestrial conditions. The capillary number is a measure of the free surface deformability. A vanishing capillary number, which can be achieved in the limit of large surface tension coefficient σ_0, corresponds to a planar interface.

In Sec. III, the governing system, which now consists of Eqs. (2.14)–(2.21), is analyzed.

III. ASYMPTOTIC ANALYSIS

A. Simplified system

The continuity equation (2.3) is removed from the formulation by introducing the general representation for a solenoidal vector field. This representation takes into account the fact that, in this case, convection does not generate a mean flow,

$$\mathbf{u}=\boldsymbol{\nabla}\times(\boldsymbol{\nabla}\times\phi\mathbf{k})+\boldsymbol{\nabla}\times\psi\mathbf{k}. \tag{3.1}$$

The components of the velocity vector field are then related to the scalar functions ϕ and ψ as follows:

$$(u,v,w)=(\phi_{XZ}+\psi_Y,\phi_{YZ}-\psi_X,-\phi_{XX}-\phi_{YY}). \tag{3.2}$$

The vertical component of the curl of the equation for momentum conservation Eq. (2.14) yields an equation for the vertical component of the vorticity $(-\nabla_H^2\psi)$,

$$P^{-1}\left[\frac{\partial}{\partial t}(\nabla_H^2\psi)-\mathbf{k}\cdot\boldsymbol{\nabla}\times(\mathbf{u}\cdot\boldsymbol{\nabla}\mathbf{u})\right]=\nabla^2(\nabla_H^2\psi), \tag{3.3a}$$

where

$$\begin{aligned}\mathbf{k}\cdot\boldsymbol{\nabla}\times(\mathbf{u}\cdot\boldsymbol{\nabla}\mathbf{u})=&(\nabla_H^2\phi)(\nabla_H^2\psi_Z)-(\nabla_H^2\phi_Z)(\nabla_H^2\psi)-(\nabla_H^2\phi_X)\\&\times[\phi_{YZZ}-\psi_{XZ}]+(\nabla_H^2\phi_Y)[\phi_{XZZ}+\psi_{YZ}]\\&-(\nabla_H^2\psi_X)[\phi_{XZ}+\psi_Y]-(\nabla_H^2\psi_Y)\\&\times[\phi_{YZ}-\psi_X].\end{aligned} \tag{3.3b}$$

The vertical component of the double curl of Eq. (2.14) yields an equation for ϕ,

$$\begin{aligned}P^{-1}\left[\frac{\partial}{\partial t^2}\nabla^2(\nabla_H^2\phi)+\mathbf{k}\cdot\boldsymbol{\nabla}\times(\boldsymbol{\nabla}\times\mathbf{u}\cdot\boldsymbol{\nabla}\mathbf{u})\right]=&\nabla^4(\nabla_H^2\phi)\\&-R\boldsymbol{\nabla}_H^2\theta,\end{aligned} \tag{3.4a}$$

where

$$\mathbf{k}\cdot\boldsymbol{\nabla}\times(\boldsymbol{\nabla}\times\mathbf{u}\cdot\boldsymbol{\nabla}\mathbf{u})=-\nabla_H^2\mathcal{I}+\mathcal{J}_{XZ}+\mathcal{K}_{YZ}, \tag{3.4b}$$

$$\begin{aligned}\mathcal{I}=&-(\nabla_H^2\psi_X)[\phi_{XZ}+\psi_Y]-(\nabla_H^2\psi_Y)[\phi_{YZ}-\psi_X]+(\nabla_H^2\psi)\\&\times(\nabla_H^2\psi_Z),\end{aligned} \tag{3.4c}$$

$$\begin{aligned}\mathcal{J}=&[\phi_{XZ}+\psi_Y][\phi_{XZ}+\psi_Y]_X+[\phi_{YZ}-\psi_X][\phi_{XZ}+\psi_Y]_Y\\&-(\nabla_H^2\psi)[\phi_{XZ}+\psi_Y]_Z,\end{aligned} \tag{3.4d}$$

$$\begin{aligned}\mathcal{K}=&[\phi_{XZ}+\psi_Y][\phi_{YZ}-\psi_X]_X+[\phi_{YZ}-\psi_X][\phi_{YZ}-\psi_X]\\&\times[\phi_{YZ}-\psi_X]_Y-(\nabla_H^2\psi)[\phi_{YZ}-\psi_X]_Z.\end{aligned} \tag{3.4e}$$

The equation for the conservation of energy, Eq. (2.15), reduces to

$$\frac{\partial\theta}{\partial t}+\boldsymbol{\nabla}_H D\phi\cdot\boldsymbol{\nabla}_H\theta-\boldsymbol{\nabla}_H^2\phi D\theta+\theta_X\psi_Y-\psi_X\theta_Y+\nabla_H^2\phi=\nabla^2\theta, \tag{3.5}$$

where the symbol D stands for $\partial/\partial Z$. Finally, an equation for the pressure is derived by considering the vertical component of Eq. (2.14),

$$\begin{aligned}Dp=&R\theta-\nabla^2(\nabla_H^2\phi)-P^{-1}\left[\frac{\partial}{\partial t}(-\nabla_H^2\phi)\right.\\&-(\phi_{XZ}+\psi_Y)\nabla_H^2(\phi_X)-(\phi_{YZ}-\psi_X)\nabla_H^2(\phi_Y)\\&\left.+\nabla_H^2(\phi_Z)(\nabla_H^2\phi)\right].\end{aligned} \tag{3.6}$$

The boundary conditions on the velocity translate into the following for the newly defined variables:

$$\phi=D\phi=\psi=0 \quad \text{on} \quad Z=0, \tag{3.7}$$

and, at the free surface located at $Z=1+\eta$,

$$\begin{aligned}&p-GP\eta+(R/2)\eta^2+(2/N)[(\boldsymbol{\nabla}_H\eta\cdot\boldsymbol{\nabla}_H)^2(D\phi)\\&\quad-\boldsymbol{\nabla}_H(D^2\phi-\nabla_H^2\phi)\cdot\boldsymbol{\nabla}_H\eta-\nabla_H^2(D\phi)]\\&\quad+(2/N)[\psi_{XY}(\eta_X^2-\eta_Y^2)+\eta_Y\psi_{XZ}-\eta_X\psi_{YZ}\\&\quad+\eta_X\eta_Y(\psi_{YY}-\psi_{XX})]\\&=N^{-3/2}\nabla_H^2\eta[1/C+M(\eta-\theta)],\end{aligned} \tag{3.8}$$

$$\begin{aligned}&(1/N)[-2\phi_{XXZ}\eta_X(1+\eta_Y^2)-2\eta_Y(1+\eta_Y^2-\eta_X^2)\phi_{XYZ}\\&\quad+(\phi_{XZZ}-\nabla_H^2\phi_X)(1+\eta_Y^2-\eta_X^2)+2\eta_X\eta_Y^2\phi_{YYZ}\\&\quad-2\eta_X\eta_Y(\phi_{ZZY}-\nabla_H^2\phi_Y)-2\eta_X\nabla_H^2\phi_Z]+(1/N)\\&\quad\times[-2(1+\eta_Y^2)\eta_X\psi_{XY}-2\eta_Y(1+\eta_Y^2-\eta^2)(\psi_{YY}-\psi_{XX})\\&\quad+(1+\eta_Y^2-\eta_X^2)\psi_{YZ}-2\eta_X\eta_Y^2\psi_{XY}+2\eta_X\eta_Y\psi_{XZ}],\\&=M[-\theta_X(1+\eta_Y^2)+\eta_X\eta_Y\theta_Y-\eta_X\theta_Z],\end{aligned} \tag{3.9}$$

$$\begin{aligned}&N^{-1/2}[-2\eta_X\phi_{XYZ}-2\eta_Y\phi_{YYZ}+(1-\eta^2)(\phi_{YZZ}-\nabla_H^2\phi_Y)\\&\quad-(\phi_{ZZX}-\nabla_H^2\phi_X)\eta_X\eta_Y-2\eta_Y\nabla_H^2\phi_Z-\eta_X\psi_{YY}-\psi_{XX}\\&\quad+2\eta_Y\psi_{XY}-(1-\eta_Y^2)\psi_{XZ}-\eta_X\eta_Y\psi_{YZ}]\\&=M(\eta_Y-\theta_Y-\eta_Y\theta_Z)\end{aligned} \tag{3.10}$$

$$\frac{\partial\eta}{\partial t}+\boldsymbol{\nabla}_H\eta\cdot\boldsymbol{\nabla}_H\phi_Z=-\nabla_H^2\phi+\psi_X\eta_Y-\eta_X\psi_Y. \tag{3.11}$$

B. Evolution equation

The fluid under consideration is sandwiched between a top air layer and a lower plate, both of which are assumed much poorer heat conductors than the fluid itself, i.e., $\beta=\beta'\ll 1$. It is a well known fact that under these assumptions the onset of convection is stationary, and that the regular convective cells that appear at onset have very long wavelengths. Proctor [13] has shown that this situation is amenable to nonlinear analysis via long wavelength asymptotics. In the following steps, we scale the horizontal variables and time, and use a well known reduction method to solve for the various quantities. The final result will be an evolution equation for the leading order temperature. The

derivation begins with the introduction of a small positive perturbation parameter $\epsilon \ll 1$ and the slow variables

$$(X,Y)=(x,y)/\epsilon^2, \quad z=Z \quad \text{and} \quad t=\tau/\epsilon^4, \tag{3.12}$$

while the control parameters R and M, and the Biot number β' are scaled as

$$R=R_0+R_2\epsilon^2, \quad M=M_0+M_2\epsilon^2, \quad \beta'=\hat{\beta}\epsilon^4, \tag{3.13}$$

where R_2, M_2, and $\hat{\beta}$ are all quantities of order unity. The convective variables as well as the interface are expanded in powers of ϵ^2 since only even order derivatives with respect to the horizontal variables appear in the equations,

$$[\theta,\phi,\psi,p]=[\theta_0,\phi_0,\psi_0,p_0]+\epsilon^2[\theta_2,\phi_2,\psi_2,p_2]+\cdots,$$
$$\eta=\epsilon^2\zeta+\cdots. \tag{3.14}$$

In order to cover a wide range of experimental situations, several scalings for the Galileo, capillary, and Prandtl numbers are considered, namely $G=O(\epsilon^{-2})$ and $G=O(1)$, $C=O(1)$ and $C=O(\epsilon^4)$, and $P=O(\epsilon^{-4})$, $P=O(\epsilon^{-2})$, and $P=O(1)$.

Before proceeding with the solution, one more simplification is in order, namely the boundary conditions describing the tangential stresses balance at the free surface [Eqs. (3.9) and (3.10]. If Eq. (3.9) is differentiated with respect to X and Eq. (3.10) with respect to Y, and the resulting expressions summed up, keeping in mind the appropriate scalings Eqs. (3.12) and (3.13), the following simplified boundary conditions at $z=1$ will result (∇_h being the horizontal gradient in the variables x and y):

$$\nabla_h^2(D^2\phi_0)=-M_0\nabla_h^2\theta_0, \tag{3.15}$$

$$\nabla_h^2(D^2\phi_2)=-\zeta\nabla_h^2(D^3\phi_0)+M_0\nabla_h^2\zeta$$
$$-M_0[\nabla_h^2\theta_2-M_0\zeta\nabla_h^2(D\theta_0)]+\nabla_h^2\zeta$$
$$-M_0\nabla_h\zeta\cdot\nabla_h(D\theta_0)-M_2\nabla_h^2\theta_0. \tag{3.16}$$

The horizontal and temporal scalings Eq. (3.12) and the scalings for the dimensionless parameters Eq. (3.13) are substituted into the governing set of equations and boundary conditions Eqs. (3.3)–(3.11), and the variables are then expanded following Eq. (3.14). By equating similar powers of ϵ, a hierarchy of boundary-value problems is obtained. The leading order problems for the perturbations of temperature and velocity are

$$D^2\theta_0=0 \quad \text{subject to} \quad D\theta_0=0 \text{ at } z=0 \text{ and } 1 \tag{3.17}$$

and

$$D^4\phi_0=R_0\theta_0, \tag{3.18a}$$

subject to

$$\phi_0(0)=D\phi_0(0)=\phi_0(1)=0,$$
$$\nabla_h^2[D^2\phi_0(1)+M_0\theta_0]=0. \tag{3.18b}$$

The first order contribution to the vertical component of vorticity satisfies

$$D^2(\nabla_h^2\psi_0)=0 \quad \text{subject to} \quad \nabla_h^2\psi_0(0)=D(\nabla_h^2\psi_0)(1)=0. \tag{3.19}$$

The boundary condition for ψ_0 at the free surface is derived as follows: differentiate Eq. (3.9) with respect to Y and Eq. (3.10) with respect to X, then subtract the latter from the former expression to obtain

$$D(\nabla_h^2\psi_0)(1)=0. \tag{3.20}$$

The leading order equation for the pressure is

$$Dp_0=R_0\theta_0. \tag{3.21}$$

The boundary condition associated with equation (3.21), which is given by Eq. (3.8), depends on the scalings adopted for the capillary, Galileo, and Prandtl numbers. They are the following ones. First: for intermediate Prandtl numbers, we find it necessary to let $P=O(1)$, and consider three possible scalings for the Galileo and Capillary numbers, namely (1) $C=O(\epsilon^4)$ and $G=O(\epsilon^{-2})$, (2) $C=O(\epsilon^4)$ and $G=O(1)$, and (3) $C=O(1)$ and $G=O(\epsilon^{-2})$. Second: for large Prandtl numbers, we let $P=O(\epsilon^{-2})$, and consider the case $G=O(1)$ and $C=O(\epsilon^4)$. Third: for very large Prandtl numbers, we let $P=O(\epsilon^{-4})$ and consider the case $C=O(\epsilon^4)$ and $G=O(1)$. The boundary condition for the pressure at $z=1$ takes one of these forms. For small to moderately large Prandtl numbers, we have (the hat denotes order one quantities)

$$\text{case 1:} \quad p_0(1)=-\hat{G}\hat{P}\zeta-(1/\hat{C})\nabla_h^2\zeta, \tag{3.22a}$$

$$\text{case 2:} \quad p_0(1)=-(1/\hat{C})\nabla_h^2\zeta, \tag{3.22b}$$

$$\text{case 3:} \quad p_0(1)=-\hat{G}\hat{P}\zeta. \tag{3.22c}$$

For $P=O(\epsilon^{-2})$ and $O(\epsilon^{-4})$, $p_0(1)$ is described by Eqs. (3.22a) and (3.22c), respectively. Other scalings, such as $G<O(1)$, require that we take the calculations at very high order in the perturbation parameter. Another possibility, which leads to $[G<O(1)]$, arises when the fluid layer is a thin film. This case can be investigated using lubrication theory to derive an evolution equation for the film thickness (See Davis [14]). The approach used in the present paper limits us to consider only the cases described by Eqs. (3.22a), (3.22b), and (3.22c).

Straightforward solution of the problems defined by Eqs. (3.17)–(3.22) yields

$$\theta_0=F(x,y,\tau), \quad \psi_0=0, \quad p_0=R_0Fz+K, \tag{3.23}$$

where K is an integration constant, and

$$\phi_0=\left[\left(\frac{R_0}{24}z^4-\left(\frac{M_0}{4}+\frac{5R_0}{48}\right)z^3+\left(\frac{M_0}{4}+\frac{R_0}{16}\right)z^2\right]F. \tag{3.24}$$

The order ϵ^2 for the conservation of heat equation (3.5) and corresponding boundary conditions Eqs. (2.5) and (2.21) reduces to

$$D^2\theta_2=[P(z)-1]\nabla_h^2F-\frac{dP}{dz}|\nabla_hF|^2, \tag{3.25}$$

subject to

$$D\theta_2=0 \quad \text{on } z=0 \text{ and } 1, \tag{3.26}$$

where $P(z)$ is the polynomial between brackets in Eq. (3.24).

The application of the solubility condition to the nonhomogeneous boundary value problem, Eqs. (3.25) and (3.26), leads to the following expression for the critical Rayleigh and Marangoni numbers R_0 and M_0:

$$\frac{R_0}{320}+\frac{M_0}{48}=1. \tag{3.27}$$

Let $m=M_0/48$, from which $R_0=320(1-m)$; then the parameter m varies between the limits $m=0$ (for purely buoyancy-driven convection) and $m=1$ (for purely surface-tension-driven flow). In terms of the recently defined parameter m, Eq. (3.24) takes the form

$$\phi_0=[\tfrac{40}{3}(1-m)z^4+\tfrac{1}{3}(64m-100)z^3+(20-8m)z^2]F. \tag{3.28}$$

Proceeding to the next power in ϵ^2, we find

$$\begin{aligned}\theta_2=&-\tfrac{1}{90}[40(m-1)z^6+(150-96m)z^5+(60m-150)z^4\\&+45z^2]\nabla_h^2F-\tfrac{1}{3}[8(1-m)z^5+(25-16m)z^4\\&+4(2m-5)z^3]|\nabla_hF|^2+L(x,y),\end{aligned} \tag{3.29}$$

where L is an arbitrary function of x and y. The solutions ϕ_2 and ψ_2 are obtained in a similar fashion. These lengthy expressions are not displayed in this paper.

The problem under consideration is a free boundary problem, since the shape of the air-liquid interface is *a priori* unknown. A relation between the leading orders of the interface deformation and the pressure is given by Eq. (3.23), and one of the equations (3.22a), (3.22b) or (3.22c). For small to moderately large Prandtl numbers, we have the following possibilities:

$$\text{case 1:} \quad p_0=R_0(z-1)F+\hat{G}\zeta+(1/\hat{C})\nabla_h^2\zeta, \tag{3.30a}$$

$$\text{case 2:} \quad p_0=R_0(z-1)F+(1/\hat{C})\nabla_h^2\zeta, \tag{3.30b}$$

$$\text{case 3:} \quad p_0=R_0(z-1)F+\hat{G}\zeta. \tag{3.30c}$$

Equation (3.30a) is obtained for the case of a moderately large Prandtl number, and (3.30c) for the very large Prandtl number case.

Furthermore, if the X component of Eq. (2.14) is differentiated with respect to X, and the Y component with respect to Y, and the results added, a relation between pressure and the velocity is obtained. At leading order, this expression takes the form

$$\nabla_h^2p_0=D^3(\nabla_h^2\phi_0). \tag{3.31}$$

The compatibility condition Eq. (3.31) is then combined with one of the equations (3.30) to yield an expression for the interface deformation. For $P=O(1)$, we find

$$\text{case 1:} \quad \hat{G}\hat{P}\zeta+\frac{1}{\hat{C}}\nabla_h^2\zeta=(120-192m)F, \tag{3.32a}$$

$$\text{case 2:} \quad \frac{1}{\hat{C}}\nabla_h^2\zeta=(120-192m)F, \tag{3.32b}$$

$$\text{case 3:} \quad \hat{G}\hat{P}\zeta=(120-192m)F. \tag{3.32c}$$

The interface deflection is described by Eqs. (3.32a) and (3.32c) for the cases of large and very large Prandtl numbers, respectively.

It is finally established, by application of the solubility condition for ϕ_4 in the order ϵ^4 of Eq. (3.5), that the sought evolution equation for the (scaled) planform function $f(x,y,\tau)$ written in reduced canonical form is

$$\begin{aligned}\frac{\partial f}{\partial\tau}=&-\nabla_h^4f-2\nabla_h^2f-\beta f-\boldsymbol{\nabla}_h\cdot\boldsymbol{\nabla}_hf|\boldsymbol{\nabla}_hf|^2\\&-\frac{a_2}{\sqrt{a_8a_3}}\boldsymbol{\nabla}_h\cdot\boldsymbol{\nabla}_hf(\nabla_h^2f)-\frac{a_9}{\sqrt{a_8a_3}}\nabla_h^2|\nabla_hf|^2-\frac{a_6}{\sqrt{a_8a_3}}\mathcal{F}_1\\&-\frac{a_5}{\sqrt{a_8a_3}}\mathcal{F}_3-\frac{a_7}{\sqrt{a_8a_3}}\mathcal{F}_2+m\left(\frac{a_3}{a_8}\right)^{1/2}\nabla_h^2\zeta\\&-a_1\left(\frac{a_8}{a_3}\right)^{1/2}\boldsymbol{\nabla}_h\cdot(\zeta\boldsymbol{\nabla}_hf)-a_{10}\zeta\nabla_h^2f-a_{11}\boldsymbol{\nabla}_h\zeta\cdot\boldsymbol{\nabla}_hf\\&-a_{12}\sqrt{a_8a_3}[\boldsymbol{\nabla}_hf\times\langle\boldsymbol{\nabla}_h\psi_2\rangle]\cdot\mathbf{k},\end{aligned} \tag{3.33a}$$

where angle brackets denote the average over the depth of the fluid layer, and where $\langle\psi_2\rangle$ satisfies the Poisson equation

$$\nabla_h^2(\langle\psi_2\rangle)=f_y\nabla_h^2(f_x)-f_x\nabla_h^2(f_y). \tag{3.33b}$$

The leading order interface deformation ζ satisfies one of the equations (3.32). The other symbols that appear in Eq. (3.33a) are defined as follows:

$$\mathcal{F}_1=(f_{xy})^2+(f_{yy})^2+(f_{xx})^2-f_{xx}f_{yy}, \tag{3.33c}$$

$$\mathcal{F}_2=f_yf_{xxy}-f_yf_{yyy}+f_xf_{xxx}-f_xf_{xyy}, \tag{3.33d}$$

$$\mathcal{F}_3=(\nabla_h^2f)^2-\boldsymbol{\nabla}_hf\cdot\boldsymbol{\nabla}_h(\nabla_h^2f), \tag{3.33e}$$

$$a_1=(16m+20)/3,\quad a_2=(4m+5)/90,$$

$$a_3=(128m^2-40m+3800)/2835,\quad a_5=5(1-m)/126P,$$

$$a_6=(16m^2+60m+50)/315P,$$

$$a_7=-(16m^2+85m+25)/315P,$$

$$a_8=-(241m^2-64m-870)/10\ 395,$$

$$a_9=(40m^2+303m+35)/630,\quad a_{10}=(5-2m),$$

$$a_{11}=(4m+5)/2,$$

$$a_{12}=-(1024m^2+1300m+6100)/945P. \qquad (3.34)$$

Since both F and ζ are scaled by the same factor, the interface deflection is represented by equations (3.32), with F replaced by f. This derivation is valid for moderate Prandtl numbers. For large Prandtl numbers, the vertical component of the vorticity becomes trivial, and the resulting evolution equation takes the form (3.33a) without the terms in front of the coefficients a_5, a_6, a_7, and a_{12}. The limit of the very small Prandtl number, which requires a different derivation for the evolution equation, is beyond the scope of the analysis.

In Sec. IV, the stability of the flow pattern in the form of hexagons, and the corresponding interface deflection, are examined directly from the evolution equation (3.33).

IV. ANALYSIS OF THE FLOW PATTERN AND OF THE FREE SURFACE DEFLECTION

A. Stability of the hexagonal flow pattern

The regular convective patterns of rolls, squares, or hexagons that are observed experimentally are only a subset of the solution manifold of Eq. (3.33), which consists of regular and also polygonal solutions. A complete analysis of the preferred planform of convection can be carried out directly from the evolution equation using techniques from equivariant bifurcation theory (Knobloch [15]). However, we shall limit this investigation to the case of the hexagonal planform, since it is the pattern that is commonly observed in the experiments. The deviation from linear threshold, which is determined by R_2 and M_2 in Eq. (3.13), is a free parameter in the analysis. The calculations show that the deviation from threshold is expressed by a relation between R_2 and M_2 that is similar to Eq. (3.27), namely $\Upsilon=R_2/320+M_2/48$. For simplicity in the calculations, we choose Υ so that the linear part is as shown in Eq. (3.33a).

A linear stability analysis of Eq. (3.33) reveals that the trivial state is stable for $\hat{\beta}>1$, and becomes unstable to a cellular regime having a wavelength 2π when $\hat{\beta}<1$. In this section, we seek the nonlinear solutions in the vicinity of the bifurcation point $\hat{\beta}=1$ using a standard approach (see Ref. [15]). For this purpose, we define a positive perturbation parameter $\gamma\ll 1$, and let

$$\hat{\beta}=1-\gamma\beta_1-\gamma^2\beta_2+\cdots,\quad s=\gamma^2\tau \qquad (4.1)$$

and

$$f=\gamma f_1+\gamma^2 f_2+\gamma^3 f_3+\cdots. \qquad (4.2)$$

Expansions (4.1) and (4.2) are substituted into the evolution equation, and the resulting sequence of problems solved. At leading order in γ, the solution is the planform for a hexagonal pattern

$$f_1=\mathcal{A}(s)\left[\cos(y)+2\ \cos\left(\frac{\sqrt{3}}{2}x\right)\cos\left(\frac{y}{2}\right)\right]. \qquad (4.3)$$

At the next order in γ, the solubility condition yields an ordinary differential equation for the amplitude $A(s)$. Without loss of generality, we have added a cubic term in order to insure the saturation of the amplitude [16],

$$\frac{d\mathcal{A}}{ds}=\beta_1\mathcal{A}+\omega\mathcal{A}^2-\mathcal{A}^3. \qquad (4.4)$$

We suppose that the interface shape conforms to the flow pattern so that $\zeta=Sf$, where S is a constant which depends on m, P, G, and C. For $P=O(1)$, ω takes the form

$$\omega=[-2a_2+2a_9-a_6-6a_5+a_7+2Sa_1a_8-2Sa_{11}(a_8a_3)^{1/2}+4Sa_{10}(a_8a_3)^{1/2}]/[4(a_8a_3)^{1/2}], \qquad (4.5a)$$

while for $P\geqslant O(\epsilon^{-2})$, we have

$$\omega=[-2a_2+2a_9+2Sa_1a_8-2Sa_{11}(a_8a_3)^{1/2}+4Sa_{10}(a_8a_3)^{1/2}]/[4(a_8a_3)^{1/2}]. \qquad (4.5b)$$

Note that the parameter β_1 measures the deviation from the critical value $\beta=1$, and that the sign of ω will determine the character of the bifurcation at threshold. The fixed points of Eq. (4.4) are given by

$$\mathcal{A}=0,\quad \mathcal{A}^+=(\omega/2)+\sqrt{(\omega^2/4)+\beta_1},$$

$$\mathcal{A}^-=(\omega/2)-\sqrt{(\omega^2)/4+\beta_1}, \qquad (4.6)$$

and are illustrated in the bifurcation diagram Fig. 2. The steady states are plotted as functions of the parameter β_1. The trivial solution becomes unstable through a transcritical bifurcation at $\beta_1=0$ which represents the linear threshold. The bifurcated solutions consist of four branches: (1) the positive part of $\mathcal{A}^+$, (2) the negative part of $\mathcal{A}^-$, (3) the negative part of $\mathcal{A}^+$, and (4) the positive part of $\mathcal{A}^-$. The first two branches are subcritical, while the last two bifurcate supercritically. It is clear that the sign of the parameter ω is the determining factor in the stability of these bifurcated solutions. A direct stability analysis from the amplitude equation cannot isolate the stable branches. The question of stability can, however, be resolved if the results of Hadji, Safar, and Schell [12] are used. Indeed, these authors have carried a detailed weakly nonlinear stability analysis on this same problem, with the added assumptions that the fluid has an infinite Prandtl number and the free interface is nondeformable (ω is positive in this case). Their analysis reveals that, near threshold, the stable pattern consist of subcritical hexagons with upflow at their centers. To show that this flow pattern is represented by $\mathcal{A}^+$, it suffices to determine the direction in which the fluid flows at the center of the hexa-

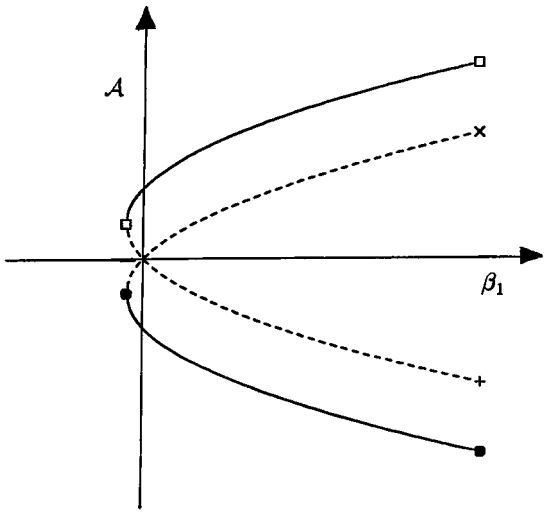

FIG. 2. Plot of the amplitude $\mathcal{A}$ as a function of the bifurcation parameter β_1. Of the four branches, two are subcritical, namely $\mathcal{A}^+$ [□] and $\mathcal{A}^-$(●). The two unstable supercritical branches are shown with the symbols (×) and (+).

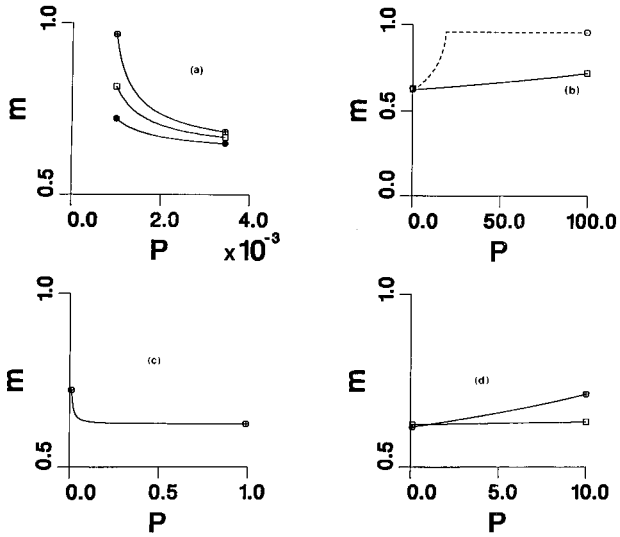

FIG. 3. Plot of m_c as a function of the Prandtl number P for (a) case (1) ($P \ll 1$), $\hat{G}=1$, $\hat{C}=4.5$ (⊗), $\hat{C}=6.0$ (□), and $\hat{C}=10$ (●); (b) case (1) (large P), $\hat{C}=1$, $\hat{G}=1$ (continuous line), and $\hat{G}=10$ (dotted line); (c) case (2), with $\hat{G}=1$ and $\hat{C}=1$; and (d) case (2), with $\hat{C}=1.3$, $\hat{G}=1$ (□), and $\hat{G}=10$ (⊗). For all cases considered, we have not detected a root to Eq. (4.5) for $P \leqslant 0.001$ ($\omega<0$) or $P>200$ ($\omega>0$).

gons using an order of magnitude analysis. Consider the leading order in ϵ for the vertical component of the fluid velocity. This is given by Eqs. (3.2) and (3.28),

$$\mathbf{u}\cdot\mathbf{k}=w=-\nabla_H^2\phi_0=-P(z)\nabla_H^2 f, \tag{4.7}$$

which at leading order in γ yields

$$w=-P(z)\nabla_H^2 f_1=\gamma P(z) f_1. \tag{4.8}$$

The fluid velocity at the center of the cell is then $w=P(z)\gamma\mathcal{A}$. Given that the polynomial $P(z)$ has no sign change in the interval $0\leqslant z\leqslant 1$, it follows that $\mathrm{sgn}(w)=\mathrm{sgn}(\gamma\mathcal{A})$. Consequently, the branch $\mathcal{A}^+$ corresponds to hexagons with upflow at their centers (upflow hexagons) and $\mathcal{A}^-$ corresponds to hexagons with down flow at their centers (downflow hexagons). For $\omega<0$, it suffices to multiply both sides of Eq. (4.4) by (-1) to deduce that the branch corresponding to $-\mathcal{A}^+$ (i.e., $\mathcal{A}^-$) is then the stable solution. This solution represents subcritical hexagons with downflow at their centers. The two supercritical branches, the negative part of $\mathcal{A}^+$ and the positive part of $\mathcal{A}^-$, are unstable.

The variation of ω with m and P is depicted in Fig. 3. It is found that the sign of ω depends primarily on the parameters m and P and on the relation between the interface deflection ζ and the temperature perturbation f. The curves shown in Fig. 3 are obtained by determining the roots m_c of the function $\omega(m)$ as a function of the Prandtl number, and for a selected set of values of the Galileo and capillary numbers. The numerical task of determining the roots of ω is accomplished by using a bisection method. Three possible scenarios are uncovered: (1) For small Prandtl numbers, ω is negative for $0\leqslant m\leqslant 1$; (2) for large Prandtl numbers, ω is positive for $0\leqslant m\leqslant 1$; and (3) for intermediate Prandtl numbers, ω has a single root, m_c, whose numerical value depends on P, G, and C. The plots of m_c that are depicted in

TABLE I. (a) Stable flow patterns and interface deflection at the center of the hexagon for the case described by Eq. (3.33a) with $\hat{G}\hat{C}\hat{P}>1$. (b) Stable flow patterns and interface deflection at the center of the hexagon for the case described by Eq. (3.33a) with $\hat{G}\hat{C}\hat{P}<1$.

	(a)		
	$0\leqslant m\leqslant 0.625$	$0.625\leqslant m\leqslant m_c$	$m_c<m\leqslant 1$
Pattern	Upflow hexagons	Upflow hexagons	Downflow hexagons
Interface deflection	convex (Elevation)	concave (Depression)	convex (Elevation)
	(b)		
	$0\leqslant m\leqslant 0.625$	$0.625\leqslant m\leqslant m_c$	$m_c<m\leqslant 1$
Pattern	Downflow hexagons	Downflow hexagons	Upflow hexagons
Interface deflection	convex (Elevation)	concave (Depression)	convex (Elevation)

TABLE II. Stable flow patterns and interface deflection at the center of the hexagon for the case described by Eq. (3.33b).

	$0 \leqslant m \leqslant 0.625$	$0.625 \leqslant m \leqslant m_c$	$m_c < m \leqslant 1$
Pattern	Downflow hexagons	Downflow hexagons	Upflow hexagons
Interface deflection	convex (Elevation)	concave (Depression)	convex (Elevation)

Fig. 3 divide the parameter space into two regions: in one region, $\omega > 0$, the flow pattern consists of subcritical upflow hexagons, and in the other region, $\omega < 0$, the preferred pattern is that of subcritical downflow hexagons.

B. Analysis of the free surface deflection

We now turn to the discussion of the free surface morphology. As pointed out above, several relations between the leading orders of interface deflection and temperature perturbation, namely Eqs. (3.32a)–(3.32c), are derived. These relations are obtained by considering various experimental situations which depend on the relative magnitudes of the Galileo, Prandtl, and capillary numbers. In the following, we will show how the sign of the interface deflection is determined by considering the case represented by Eq. (3.32a). This equation admits a solution having the same horizontal periodicities as f, so that $\nabla_h^2 \zeta = -\zeta$. We thus obtain

$$\zeta = \frac{(120 - 192m)\hat{C}}{\hat{G}\hat{C}\hat{P} - 1} f, \tag{4.9}$$

provided that $\hat{G}\hat{C}P \neq 1$. At leading order in γ, the planform function satisfies $f = \gamma f_1$, where f_1 is given by Eq. (4.3). This implies that the first order in γ for ζ, evaluated at the center of the hexagonal cell, is described by

$$\zeta = \frac{(120 - 192m)\hat{C}}{\hat{G}\hat{C}\hat{P} - 1} \gamma \mathcal{A}. \tag{4.10}$$

The sign of ζ is then determined by sign analysis of the various factors that appear in Eq. (4.10). The sign of $\gamma\mathcal{A}$ is determined from the stability results. Here it is found that a critical value m_c exists above which ω is positive, and below which it is negative. It then follows that upflow hexagons ($\mathcal{A}^+$) are stable for $m < m_c$ and downflow hexagons (i.e., $\mathcal{A}^-$) are stable for $m > m_c$. For instance, for the case $\hat{G}\hat{C}\hat{P} > 1$, $\mathrm{sgn}(\zeta) = \mathrm{sgn}(\gamma\mathcal{A})$ if $m < 120/192 = 0.625$, and $\mathrm{sgn}(\zeta) = -\mathrm{sgn}(\gamma\mathcal{A})$ if $m > 0.625$. The results of the analysis of the sign of ζ from Eq. (4.10) are summarized in Table I(a). Note that the interface is convex for both buoyancy-driven (BD) flows (m near 0) and surface-tension-driven (STD) flows (m near 1). The interface is concave in a small range of the coupling parameter, $0.625 < m < m_c$. Since only elementary modifications of the above arguments are applied to the analysis of the sign of ζ for the other cases, we omit the details and display only a summary of the results in Tables I(b)–IV. Note that the interface is elevated at the center of the cell for all cases depicted in Tables I(a)–III for either BD or STD flows. These predictions have not been revealed before due to the fact that the theoretical study of Perez-Garcia *et al.* [9] is linear, and thus does not include the influence of the stable flow pattern on the interface deflection; and the experimental work of Cerisier *et al.* [10] has been carried out using silicone oil as the working fluid. An estimation of the physical parameters for a 3-mm layer of 100-CS silicone oil using data from Ref. [17] yields the following: $P \approx 913$, $C \approx 0.007$, and $G \approx 8.8$. Note that $(C)^{1/4} \sim (P)^{-1/4}$. Accordingly, the scalings $C = O(\epsilon^4)$, $G = O(1)$, and $P = O(\epsilon^{-4})$ are appropriate for the description of this experiment. Only for this particular case, are the results of our analysis summarized in Table IV, in agreement with the experimental findings of Cerisier *et al.* [10].

V. REMARKS AND CONCLUSION

In order to understand the influence of the various parameters and of the interfacial deformations on the stability of the motionless state, we will examine the stability of the trivial solution directly from the unscaled evolution equation, whose linearized part is

$$\frac{\partial F}{\partial \tau} = -a_8 \nabla_h^4 F - \Upsilon \nabla_h^2 F - \beta F + m \left(\frac{a_3}{a_8} \right)^{1/2} \nabla_h^2 \zeta. \tag{5.1}$$

There are solutions

$$F(x,y,\tau) = \exp(\tilde{\omega}\tau + l\mathbf{k}\cdot\mathbf{r}) \quad \text{and} \quad \zeta = SF, \tag{5.2}$$

with

TABLE III. Stable flow patterns and interface deflection at the center of the hexagon for the case described by Eq. (3.33c).

	$0 \leqslant m \leqslant 0.625$	$0.625 \leqslant m \leqslant 1$
Pattern	Upflow hexagons	Downflow hexagons
Interface deflection	convex (Elevation)	convex (Elevation)

TABLE IV. Stable flow patterns and interface deflection at the center of the hexagon for the case of a very large Prandtl number.

	$0 \leqslant m \leqslant 0.625$	$0.625 \leqslant m \leqslant 1$
Pattern	Upflow hexagons	Upflow hexagons
Interface deflection	convex (Elevation)	concave (Depression)

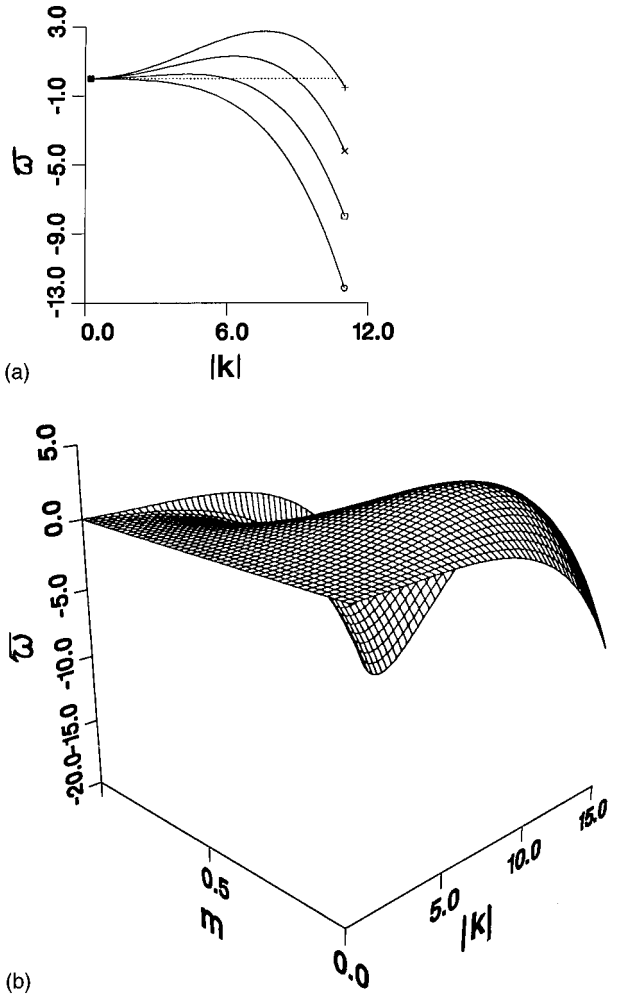

FIG. 4. (a) Plot of the growth rate $\tilde{\omega}$ as a function of the wave number $|\mathbf{k}|$ for $m=0.3$ (+), $m=0.1$ (X), $m=0.6$ (□), and $m=0.7$ (○). The interval of unstable wave numbers increases in length as m increases from 0 to about 0.3, and then decreases for $m>0.3$. There are no unstable wave numbers for $m>0.63$. (b) A surface plot of $\tilde{\omega}$ as a function of m and the wave number $|\mathbf{k}|$. Other parameters pertain to case 2.

$$\tilde{\omega}=-a_8|\mathbf{k}|^4+\left[\Upsilon-Sm\left(\frac{a_3}{a_8}\right)^{1/2}\right]|\mathbf{k}|^2-\beta. \tag{5.3}$$

The coefficients in Eq. (5.3), namely a_8, Υ, and β, and m are all positive. Thus instability ($\tilde{\omega}>0$) sets in whenever the term between brackets becomes positive. Without loss of generality, the coefficients Υ and β may be fixed arbitrarily, and the sign of $\tilde{\omega}$ investigated as a function of m. Note that instability does not occur for any wave number $|\mathbf{k}|$ when the term between brackets is negative. It is therefore clear that experimental situations for which S is positive have a stabilizing influence, while those for which S is negative have a destabilizing influence. See Figs. 4(a) and 4(b).

In deriving Eq. (4.10) for ζ, the term $(\hat{G}\hat{P}\hat{C}-1)$ appears in the denominator. If $(\hat{G}\hat{P}\hat{C}-1)$ is close to zero, then ζ can possibly be large enough to be outside the limits within which our asymptotic analysis is valid. Moreover, resonance

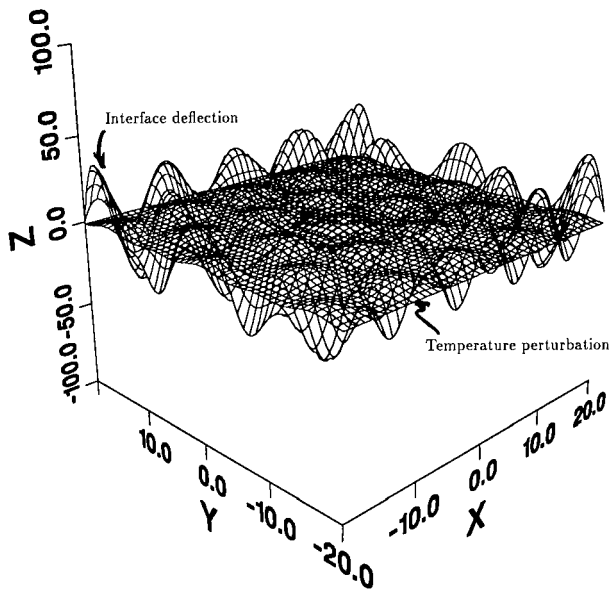

FIG. 5. Surface plots for the interface and the temperature fluctuations for the resonant case ($\hat{G}\hat{C}\hat{P}=1$) described by Eq. (3.33a) with $(120-192m)\hat{C}$ set arbitrarily to 1. Note that while the temperature profile is periodic, the interface profile is quasiperiodic.

will occur if $\hat{G}\hat{P}\hat{C}=1$ and a solution to Eq. (3.32a) will then be

$$\begin{aligned}\zeta=\mathcal{A}\{&\cos y+\cos[(\sqrt{3}x-y)/2]+\cos[(\sqrt{3}x+y)/2]\}\\&+(\mathcal{B}/4)(\sqrt{3}x-y)\sin[(\sqrt{3}x-y)/2]+(\mathcal{B}/2)y\ \sin y\\&+(\mathcal{B}/4)(\sqrt{3}x+y)\sin[(\sqrt{3}+y)/2],\end{aligned} \tag{5.4}$$

where $\mathcal{B}=(120-192m)\hat{C}\mathcal{A}$. It turns out that, in this case, the morphology of the interface does not conform to the flow pattern. A representative solution is shown in Fig. 5.

Another point worth remarking on is the fact that the interfacial deflection vanishes for $m=0.625$, and can be made extremely convex or deeply concave by varying m accordingly. Note that $m=0.625$ corresponds to a Marangoni number $M=30$ and Rayleigh number $R=120$. Again, if we make use of the data for silicone oil from Ref. [17], we find that $m=0.625$ for a layer of depth $d=4.68$ mm. The deviation from planarity is also found to increase with the amplitude of motion $\mathcal{A}$.

In conclusion, we reiterate our main result, namely the claim that in RBM convection there is upflow beneath depressions for STD flows and downflow under depressions for BD flows is *not true* in general. Our analysis showed that both the type of hexagonal patterns that appear at the onset of convection and the associated interfacial deformations depend in a complex way on the physical and control parameters as well as on the interplay between surface tension and buoyancy forces. The influence of the Prandtl number is particularly noted. Notice that from an experimental standpoint,

the Prandtl number can be varied only by changing the fluid [18]. Even though this analysis is valid only in the limit of an experimental setup that is nearly insulating, the qualitative nature of the results is not expected to be altered if the present analysis is experimentally tested in a cell having a plate of low, but finite, thermal conductance [19]. This analysis will, hopefully stimulate the development of related experiments.

[1] J. R. A. Pearson, J. Fluid Mech. **4**, 489 (1958).

[2] H. Bénard, Rev. Gen. Sci. Pures Appl. **11**, 1261 (1990).

[3] H. Jeffreys, Q. J. Mech. Appl. Math. **IV**, 283 (1951).

[4] M. J. Block, Nature **178**, 650 (1956).

[5] L. E. Scriven and C. V. Sternling, J. Fluid Mech. **19**, 321 (1964).

[6] D. A. Nield, J. Fluid Mech. **19**, 341 (1964).

[7] R. D. Benguria and M. C. Depassier, Phys. Fluids A **2**, 1123 (1989).

[8] J. R. Kraska and R. L. Sani, Int. J. Heat Mass Transfer **22**, 535 (1979).

[9] C. Perez-Garcia, J. Pantaloni, J. Ocelli, and P. Cerisier, J. Phys. **46**, 2047 (1985).

[10] P. Cerisier, C. Jamond, J. Pantaloni, and J. C. Charmet, J. Phys. **45**, 405 (1984).

[11] V. G. Levitch and V. S. Krylov, Ann. Rev. Fluid Mech. **1**, 293 (1969).

[12] L. Hadji, J. Safar, and M. Schell, J. Non-Equilib. Thermodyn. **16**, 343 (1991). The derivation of an expression for the heat transfer coefficient β' that appears in Eq. (2.21) is described in the Appendix. The derivation makes use of the experimental fact that the air layer is bounded from above by a plate. Note the following correction: H should be the plate's thickness, and D the depth of the air layer.

[13] M. R. E. Proctor, J. Fluid Mech. **113**, 469 (1981).

[14] S. H. Davis, Ann. Rev. Fluid Mech. **19**, 403 (1987).

[15] E. Knobloch, Physica D **41**, 450 (1990).

[16] P. Manneville, *Dissipative Structures and Weak Turbulence* (Academic, New York, 1990), pp. 161 and 162.

[17] E. L. Koschmeider and S. A. Prahl, J. Fluid Mech. **215**, 571 (1990). The physical properties of Silicone Oil are displayed in Table I on p. 573.

[18] M. Assenheimer and V. Steinberg [Phys. Rev. Lett. **76**, 736 (1996)] describe a method for varying the Prandtl number in a Rayleigh-Bénard convection experiment without changing the working fluid. These authors report observing domains of down-hexagons coexisting with domains of up-flow hexagons. The present analysis predicts boundaries in the parameter space of RBM convection that separate up-flow hexagons from down-hexagons. The possibility of coexistence is theoretically ruled out. From an experimental point of view, however, coexistence is plausible. For instance, for the experimental situation that is described by Eq. (3.32a), up-flow hexagons are predicted to occur for $\hat{G}\hat{C}\hat{P}<1$ and down-hexagons for $\hat{G}\hat{C}\hat{P}>1$. During the testing of this case, spatial nonuniformities in the physical parameters may divide the fluid cell into regions consisting of up-flow hexagons ($\hat{G}\hat{C}\hat{P}>1$) coexisting with regions of down-hexagons ($\hat{G}\hat{C}\hat{P}<1$).

[19] The experimental setup that is appropriate to our present analysis is that of a fluid layer overlying a layer of air, and bounded below by a plate whose thermal conductance is low compared to that of the fluid. In this case the critical wave number is small but not zero. The resulting convection flow is therefore not homogeneous but cellular. Consequently, the present analysis can be tested by making use of an experimental apparatus analogous to the one used by P. Le Gal, A. Pocheau, and V. Croquette [Phys. Rev. Lett. **54**, 2501 (1985)].